

# A statistical distribution texton feature for synthetic aperture radar image classification\*

Chu HE<sup>1,2</sup>, Ya-ping YE<sup>1</sup>, Ling TIAN<sup>†‡1,4</sup>, Guo-peng YANG<sup>2</sup>, Dong CHEN<sup>3</sup>

(<sup>1</sup>School of Electronic Information, Wuhan University, Wuhan 430072, China)

(<sup>2</sup>State Key Laboratory of Information Engineering in Surveying, Mapping and Remote Sensing, Wuhan University, Wuhan 430072, China)

(<sup>3</sup>School of Electronic Science and Engineering, National University of Defense Technology, Changsha 410073, China)

(<sup>4</sup>Hubei P&T Plan-Design Co., Ltd., Wuhan 430023, China)

<sup>†</sup>E-mail: lingtianwhu@126.com

Received Mar. 5, 2016; Revision accepted Sept. 4, 2016; Crosschecked Oct. 10, 2017

**Abstract:** We propose a novel statistical distribution texton (s-texton) feature for synthetic aperture radar (SAR) image classification. Motivated by the traditional texton feature, the framework of texture analysis, and the importance of statistical distribution in SAR images, the s-texton feature is developed based on the idea that parameter estimation of the statistical distribution can replace the filtering operation in the traditional texture analysis of SAR images. In the process of extracting the s-texton feature, several strategies are adopted, including pre-processing, spatial gridding, parameter estimation, texton clustering, and histogram statistics. Experimental results on TerraSAR data demonstrate the effectiveness of the proposed s-texton feature.

**Key words:** Synthetic aperture radar; Statistical distribution; Parameter estimation; Image classification  
<https://doi.org/10.1631/FITEE.1601051>

**CLC number:** TP753

## 1 Introduction


Synthetic aperture radar (SAR) images have been increasingly used for land description and scene analysis because of their high spatial resolution and operating ability for day and night (Yonezawa *et al.*, 2012). However, the well-known speckle phenomenon caused by the interaction of reflected waves from various independent scatterers within a resolution cell makes it hard to extract informative and distinguishing features for SAR image interpretation. The intensity fluctuation of texture in SAR images originates from the intrinsic spatial variability

of the scene and is usually affected by speckle noise (Fukuda, 2004). Texture analysis has been successfully applied in a variety of research areas such as remote sensing and machine vision.

Currently, a lot of feature descriptors have been generated from filtered images in classification or segmentation tasks. A time-frequency analysis algorithm proposed by Spigai *et al.* (2011) is based on a sliding bandpass filtering in the Fourier domain. The fractional Fourier transform (FRFT) is used to discover the underlying backscattering phenomenon of the objects in single-look SAR images. Gabor filtering is found suitable mainly for the images with strong texture under the assumption that the local texture regions are spatially homogeneous (Singh and Datcu, 2013). The image after the filter banks is divided into several blocks, and the feature descriptor is horizontally generated using the

<sup>‡</sup> Corresponding author

\* Project supported by the National Natural Science Foundation of China (Nos. 41371342 and 61331016) and the National Key Research and Development Program of China (No. 2016YFC0803003-01)

 ORCID: Chu HE, <http://orcid.org/0000-0003-3662-5769>

© Zhejiang University and Springer-Verlag GmbH Germany 2017

means or variances between blocks. Another kind of method is based on texton. Generally, a vector image is constructed by combining the value of each filter response with one pixel of the original image. These vectors are then quantified to generate a texton map, and further statistical strategies such as histogram counting are performed to produce the feature. Various texton-based texture descriptors have been explored in the last decades. Leung and Malik (2001) defined a two-dimensional (2D) texton as a cluster center in the filter response space, and developed it to a three-dimensional (3D) texton with representative viewpoints and lighting. Varma and Zisserman (2002; 2005) built a texton dictionary based on the statistical distribution of clustered filter responses for texture representation (VZ descriptor). Compared with Schmid (2001), Varma and Zisserman (2002; 2005) introduced a probabilistic model to capture the visual structure and the texton clustered in a higher dimensional space.

To better describe the texture information of different land-cover typologies, a lot of SAR-specific distributions have been proposed to model the statistics of amplitude or intensity data. The distribution models have demonstrated enormous potential for SAR image analysis and therefore received considerable attention. Combining data analysis of different sensors with the scattering mechanism of different land covers, the statistical distributions can be classified into heuristic distributions and theoretical distributions. Heuristic distributions come from the experience of data analysis without theoretical derivation. Current heuristic distributions (including Weibull, log-normal, and Fisher) and generalized Gamma distributions (GFD) have shown good performance in several particular cases (Krylov *et al.*, 2008). Moreover, to describe different kinds of radar data, several theoretical models have been developed from the product model and the generalized central limit theorem. The product model assumes that the observed values of SAR images are derived from the terrain radar cross section (RCS) and multiplicative speckle noise. In the homogeneous area with a constant RCS, Rayleigh distribution for single-look amplitude and square root Gamma (Nakagami) distribution for multi-look amplitude have been derived (Oliver and Quegan, 2004). While in the observation of high spatial resolution SAR images, Rayleigh distribution cannot describe the variety of the clutter's

statistic characteristic caused by a changing RCS of the target radar properly. Real experiments have indicated that heuristic distributions such as log-normal and Weibull remedy this descriptive weakness to some extent and model well for the background clutter of SAR imagery. The models based on the generalized central limit theorem assume that the sum of a set of independent and identically distributed random variables is subject to an  $\alpha$ -stable distribution (Kuruoglu and Zerubia, 2000). The real and imaginary parts of data received from the SAR system are both modeled by the symmetric  $\alpha$ -stable distribution (Kuruoglu and Zerubia, 2003), thus resulting in a heavy-tailed Rayleigh model for the amplitude distribution.

Statistical modeling has been applied well in SAR image interpretation. Since the texture is usually polluted by speckle noise, the second-order statistics has been adopted to solve the problem of binary additive mixture of Gamma law, which models the speckles and estimates the parameters of Fisher distribution (Benboudjema and Tupin, 2013). The dynamic B-spline deformable contours under the  $\mathcal{G}^0$  model were employed for boundary detection in speckled imagery by Gambini *et al.* (2006). The finite mixture models developed for SAR image classification have been proposed to adapt for different land covers. For example, a mixture of log-normal densities was adopted as a probabilistic model for the pixel intensities in both water and land classes (Silveira and Heleno, 2009). Voisin *et al.* (2010) developed a mixed component model to estimate the class-conditional probability density functions of SAR images. Statistical distributions can approximately describe the scattering characteristics of SAR images in theory, and the parameters of distributions are widely used for feature representation (He *et al.*, 2013). An exact modeling of statistical information improves the performance of SAR image processing effectively.

The filter banks of the filtering, labeling, and statistics (FLS) framework previously proposed (He *et al.*, 2008) provide a unified explanation of a series of features such as local binary pattern (LBP), its variants, scale-invariant feature transform (SIFT), and VZ by considering different filters and labeling functions in the filtering and labeling block respectively. The experimental results reveal the efficiency and capability of the FLS framework in

in-depth analysis of texture descriptors on a common background.

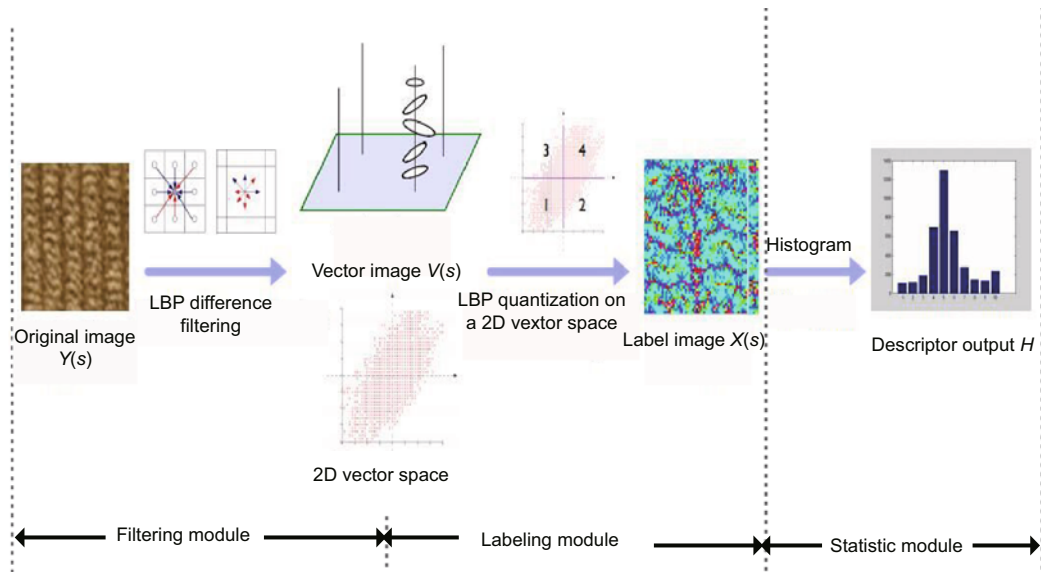
The important contributions of this paper are: (1) introducing the FLS framework into SAR image analysis, (2) using proper distributions obtained by the model selection method in Krylov *et al.* (2008) instead of the filters in the information collecting module of the framework for texture analysis, owing to the coherence of SAR imaging, and (3) applying the related algorithms of the clustering and statistical module that have been proved very effective in dealing with optical images to construct a feature descriptor of SAR images.

## 2 Distribution model selection

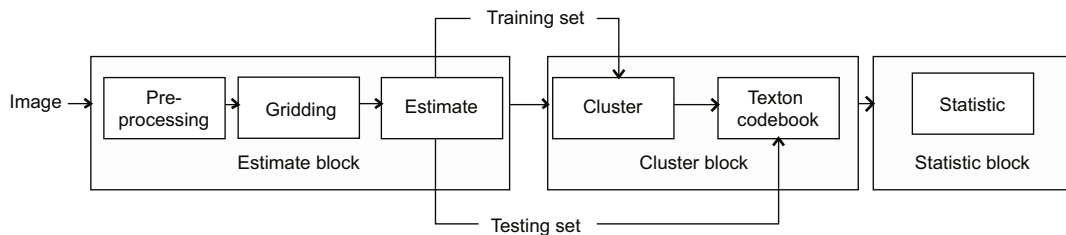
The FLS framework introduced in our previous work (He *et al.*, 2008) is a novel development of the original LBP operator which comprises information collecting, labeling, and statistic modules (Fig. 1a).

First, the input image on a rectangular pixel lattice is processed with a filter bank of the information collecting module where multi-scale and multi-direction information can be extracted. Gather the responses of the filter bank to build up a vector image. Second, obtain a label image with some labeling procedure including threshold quantization and mapping to a rotation-invariant and uniform pattern in the vector space on the labeling module. Finally, the statistics, usually a histogram count, will be performed on the labeled image to produce the export descriptor.

Instead of convolving images with a filter bank, the statistical distributions are used in the information collecting module for texture analysis, which will be described in detail in the next section. The parameters of distributions can reflect structure information and reduce the interference of speckles in SAR images. However, since SAR data can be described by different distributions, choosing optimal distributions becomes a challenge.



(a)



(b)

Fig. 1 FLS framework (a) and the proposed texture description framework for SAR images (b)

**2.1 Parameter estimation and model selection**

To develop an effective feature for SAR image interpretation, the distributions we choose should be widely used and have suitable analytic solutions for parameter estimation. Heuristic models have shown good results in several particular cases. Theoretical models can enhance the descriptive ability in dealing with different types of radar data. The Gaussian distributions with different parameters construct a mixture model to accommodate different land covers. To overcome the difficulties in choosing a suitable model, no special parametric family is adopted, and a distribution dictionary  $D=\{f_1, f_2, \dots, f_M\}$  is constructed, where  $f_i$  ( $i = 1, 2, \dots, M$ ) represents the distribution function. The statistical distribution of the SAR image is selected from a complete set of distributions. Table 1 lists the 10 distribution

functions and MoLC (method of logarithmic cumulants) equations which are involved in the considered dictionary.

**2.2 Parameter estimation method**

A proper method should be used to estimate the parameters of the distributions. There are several popular methods for parameter estimation, such as maximum likelihood (ML) (Oliver, 1986), the method of moment (MoM) (Oliver and Quegan, 2004), and MoLC (Krylov et al., 2013). The ML estimation method computes the parameter values that maximize the log-likelihood function for the observed image data. The MoM method represents the moments of the parametric probability density function (PDF) as functions of the unknown parameters and estimates the moments as sample-moment.

**Table 1 Functions and MoLC equations of the distribution in the considered dictionary  $D$**

Family	Distribution function	MoLC
Gaussian	$f_1(r/\sigma) = \frac{1}{2\sigma} \exp\left(-\frac{r}{\sigma^2}\right)$	$k_1 = \ln(2\sigma^2) + \psi(0, 1)$
Log-normal	$f_2(r/\mu, \sigma) = \frac{1}{\sqrt{2\pi}} \exp\left[-\frac{(\ln r - \mu)^2}{2\sigma^2}\right]$	$k_1 = \mu, k_2 = \sigma^2$
Weibull	$f_3(r/\mu, \eta) = \frac{\eta}{\mu^\eta} r^{\eta-1} \exp\left[-\left(\frac{r}{\mu}\right)^\eta\right]$	$k_1 = \ln \mu + \eta^{-1}\psi(0, 1), k_2 = \eta^{-2}\psi(1, 1)$
Fisher	$f_4(r/L, M, \mu) = \frac{\Gamma(L+M)}{\Gamma(L)\Gamma(M)} \frac{L}{M\mu} \frac{\left(\frac{Lr}{M\mu}\right)^{L-1}}{\left(1 + \frac{Lr}{M\mu}\right)^{L+M}}$	$k_1 = \ln \mu + (\psi(L) - \ln L) - (\psi(M) - \ln M),$ $k_2 = \psi(1, L) + \psi(1, M), k_3 = \psi(2, L) - \psi(2, M)$
Generalized Gaussian distribution (GGD)	$f_5(r/v, \sigma, k) = \frac{v}{\sigma\Gamma(k)} \left(\frac{r}{\sigma}\right)^{kv-1} \exp\left[-\left(\frac{r}{\sigma}\right)^v\right]$	$k_1 = \psi(k)/v + \ln \sigma, k_2 = \psi(1, k) + \psi(1, M),$ $k_3 = \psi(2, L) - \psi(2, M)$
Rayleigh	$f_6(r/\sigma) = \frac{r}{\sigma^2} \exp\left(-\frac{r}{2\sigma^2}\right)$	$k_1 = \ln(2\sigma^2) + \psi(0, 2)$
Nakagami	$f_7(r/L, \lambda) = \frac{2}{\Gamma(L)} (\lambda L)^L r^{2L-1} \exp(-\lambda L r^2)$	$2k_1 = \psi(0, L) - \ln \lambda - \ln L, 4k_2 = \psi(1, L)$
$K$ -root	$f_8(r/L, M, \mu) = \frac{4}{\Gamma(L)\Gamma(M)} \left(\frac{LM}{\mu}\right)^{(L+M)/2} \cdot r^{L+M-1} K_{M-L} \left[2r \left(\frac{LM}{\mu}\right)^{1/2}\right]$	$2k_1 = \ln \mu + \psi(L) - \ln L + \psi(M),$ $4k_2 = \psi(1, L) + \psi(1, M), 8k_3 = \psi(2, L) + \psi(2, M)$
Square root $\mathcal{G}^0$	$f_9(r/M, L, \mu) = \frac{2\Gamma(L+M)}{\Gamma(L)\Gamma(M)} \frac{C^L r^{2L-1}}{(1 + Cr^2)^{L+M}},$ $C = \frac{L}{M\mu}$	$k_1 = \ln(M\mu) - \ln L + \frac{1}{2} [\psi(L) - \psi(M)],$ $k_j = \left(\frac{1}{2}\right)^j [\psi(j-1, L) - (-1)^j \psi(1, M)], j = 2, 3$
Heavy-tailed Rayleigh (S $\alpha$ S)	$f_{10}(r/\alpha, \gamma) = r \int_0^\infty \rho \exp(-\gamma\rho^\alpha) J_0(\rho r) d\rho$	$\alpha k_1 = (\alpha-1)\psi(0, 1) + \ln(\gamma 2^\alpha), k_2 = \alpha^{-2}\psi(1, 1)$

$\Gamma(\cdot)$  is the Gamma function,  $\psi(\cdot)$  is the Digamma function,  $\psi(v, \cdot)$  is the  $v$ th-order polyGamma function, and  $J_0$  is the 0th-order Bessel function of the first kind

However, for the distribution families involving complicated analytical expressions, the ML method lacks attractive asymptotical properties under regularity conditions. MoM is sensitive to noise or registration faults, and has the same numerical or initialization problems as ML. MoLC employs a strategy based on the Mellin transform to compute characteristic and moment generating functions. Compared with ML and MoM, MoLC can describe the developed statistical product models more accurately and exhibit better variance properties. It proves to be a feasible and computationally fast alternative to MoM and ML for texture analysis of SAR images with speckles. Therefore, MoLC is used to estimate the distribution parameter.

MoLC is a parameter estimation method based on PDF MeLin integral transform. For a random variable  $x \in (0, +\infty)$  with the PDF  $f(x)$ , the MeLin transform is defined as

$$\phi(s) = \text{MT}[f](s) = \int_0^{+\infty} x^{s-1} f(x) dx. \quad (1)$$

Calculate the  $i$ th derivative to obtain the logarithmic moment estimation, where  $s=1$ :

$$l_i = \left. \frac{d^i \phi(s)}{ds^i} \right|_{s=1} = \int_0^{+\infty} (\ln x)^i f(x) dx, \quad i = 1, 2, \dots \quad (2)$$

We can obtain the logarithmic cumulants by giving  $\ln \phi(s)$  the same operation as follows:

$$k_i = \left. \frac{d^i \phi(s)}{ds^i} \right|_{s=1}, \quad i = 1, 2, \dots \quad (3)$$

Regarding the lower moment, the relationship between the logarithmic moment and logarithmic cumulants can be described as

$$\begin{cases} k_1 = l_1, \\ k_2 = l_2 - l_1^2, \\ k_3 = l_3 - 3l_2 l_1^2 + 2l_1^3. \end{cases} \quad (4)$$

As illustrated in Table 1, the logarithmic cumulants can be estimated according to the distribution model. The number of parameters varies from distribution to distribution, so is the meaning of the parameters. In the log-normal distribution, there are two parameters, i.e., scale parameter  $\mu$  and shape parameter  $\sigma$ . Similarly, the only parameter  $\sigma$  in Rayleigh represents the scale. As for the Weibull distribution,  $\mu$  is the scale parameter and  $\eta$  is the shape

parameter. Nakagami has two parameters, shape parameter  $\lambda$  and the other parameter  $L$  standing for the equivalent line of sight.

### 2.3 Model selection

In this study, we adopt the log-likelihood method as the selection criterion to choose the optimal distributions from  $D = \{f_1, f_2, \dots, f_M\}$ . The log-likelihood of each distribution is defined as follows:

$$L_i = \sum_{r \in Q} \ln f_i(r), \quad i = 1, 2, \dots, M, \quad (5)$$

where  $Q$  is the set of image pixels and  $f_i(\cdot)$  is the  $i$ th parametric model in the dictionary. The values of  $L_i$  are sorted in descending order.

## 3 Statistical distribution texton feature

Based on the texton feature from the framework and distribution characters of SAR images, a statistical texton (s-texton) feature is derived especially for SAR images. The s-texton algorithm consists of three processing blocks (Fig. 1b), i.e., estimation block (E-Block), cluster block (C-Block), and statistic block (S-Block). The input data is a single-band  $N \times N$  image in this study and the final output is a vector of texton numbers  $\mathbf{S}$  in the codebook, which represents the input parameters to be defined by the user based on heuristics in the image understanding system. Each stage will be described in turn with their candidate algorithms to produce an overall statistical texton feature. The process of extracting the s-texton feature is shown in Fig. 2 and will be explained in the following subsections.

### 3.1 E-Block

The estimation block contains three stages: pre-processing, gridding, and estimation (Fig. 1b).

#### 3.1.1 Pre-processing

Pre-processing is mainly to obtain the suitable distribution, which can fit the SAR image well. The distributions in the dictionary  $D = \{f_1, f_2, \dots, f_M\}$  have shown the potential for SAR image analysis. However, with this specific choice, the estimation process includes  $M=10$  distinct parametric families. We select randomly one image from each class, and

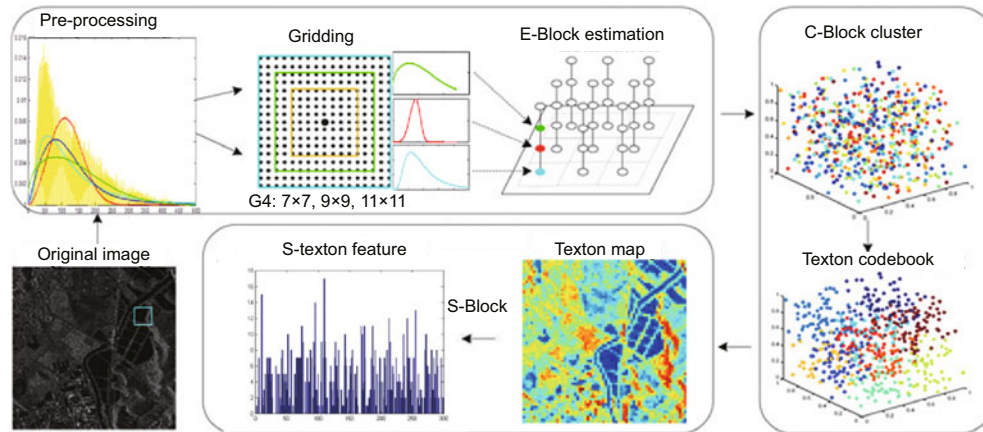


Fig. 2 Extraction process of the proposed statistical texton descriptor

then link these images together to produce a new image  $I$  modeled by the distributions in dictionary  $D$ . The parameter values of all the distributions in dictionary  $D$  are estimated by MoLC over the SAR data. Then as the selection criterion, the log-likelihood is computed for each component to obtain the optimal distributions. Several combination strategies of different estimators chosen from distribution dictionary  $D$  have been applied to construct a proper model.

### 3.1.2 Gridding

In this stage, the image is partitioned into grids. We define  $m$  as the number of grids for each pixel at a level. These grids contain neighborhoods of each pixel, so the feature extracted from them may express spatial information. Different sizes or patterns of the grid are chosen as follows:

G1–G3: A single square grid is used for each dimension of the vectors from the pre-processing stage. Each pixel is assumed to be the grid center and the grid sizes are  $5 \times 5$ ,  $9 \times 9$ , and  $13 \times 13$  for G1–G3, respectively. In this case,  $M=1$ .

G4: We use grids of different sizes to form a combined grid—a three-level grid with sizes  $7 \times 7$ ,  $9 \times 9$ , and  $11 \times 11$ . Thus, scale information is added to the grids and  $M=3$ .

G5: The neighbors in the grid are divided into four parts: left-up, left-down, right-up, and right-down. There are four grids in each direction for one subgrid and  $M=4$ . In this way, the grid contains spatial information of the image.

### 3.1.3 Estimation

In this stage MoLC is used to compute distribution parameters of each grid from the gridding sub-block to obtain a vector with length  $p \times M$ , where  $p$  is the number of parameters per distribution. We use the distributions obtained in the pre-processing stage to obtain the parameters by modeling the grid. Single distributions and multiple distributions (combination of two or more) are employed to describe the SAR image. Then parameters of the distributions in the sub-block except the boundary pixels are cascaded to produce a vector which embodies multiple types of information.

### 3.2 C-Block

This stage is aimed to cluster the vectors obtained in the E-Block to make the s-texton feature stable and flexible. In this study,  $K$ -means is used to cluster the parameters of distribution models for SAR images. As for the training set, the statistical texton codebook has not yet been generated. Therefore, the estimated vectors are clustered to form a codebook. For each test image, the corresponding estimated vector of each pixel is directly labeled by the codebook, and after the C-Block, a histogram will be established in the following S-Block stage.

### 3.3 S-Block

This block is similar to the statistic module in the FLS, where a statistic procedure will be followed on the labeled image through a histogram count. The s-texton can then be obtained.

Above all, for an image, first, set the size of image patch and choose a distribution; second, compute the distribution's parameters, and cluster by the vector of these parameters; third, connect all the patches' cluster features to form the feature of the whole image; finally, statistic for s-texton features is used for classification. Each module's setting will be presented in the following section.

## 4 Experiments

### 4.1 Experiment dataset

The TerraSAR image used in the experiments involves the area of Guangzhou Province in China detected on May 24, 2008 (UTC-Universal Time Coordinated), as shown in Figs. 3a–3c. The image data with channel VV is in the intensity field and 16-bit. The terrain varies from urban area to farmland, including seven classes: forest, hill, industry area, land, pool with bridge, river, and residential area (Fig. 3d).

Each class includes 160 sub-images sized in  $64 \times 64$ , from which 60 sub-images are used for training and the remainder for testing.

### 4.2 S-texton setup

To further assess the capabilities of different distributions, Fig. 4 shows the image histograms and the distributions estimated in the dictionary. Since the amplitude data in SAR images often exhibits heavy distribution tails, Rayleigh distribution obviously performs poorly (Fig. 4a). However, heuristic distributions such as log-normal and Weibull can overcome the descriptive weakness of the Rayleigh distribution to some extent. According to the log-likelihood method, the selected distributions are log-normal, Nakagami,  $S\alpha S$ , Weibull, and Rayleigh in descending order.

To choose the number of distributions denoted by  $N$ , the following experiments were conducted to compare the performance of a single estimator

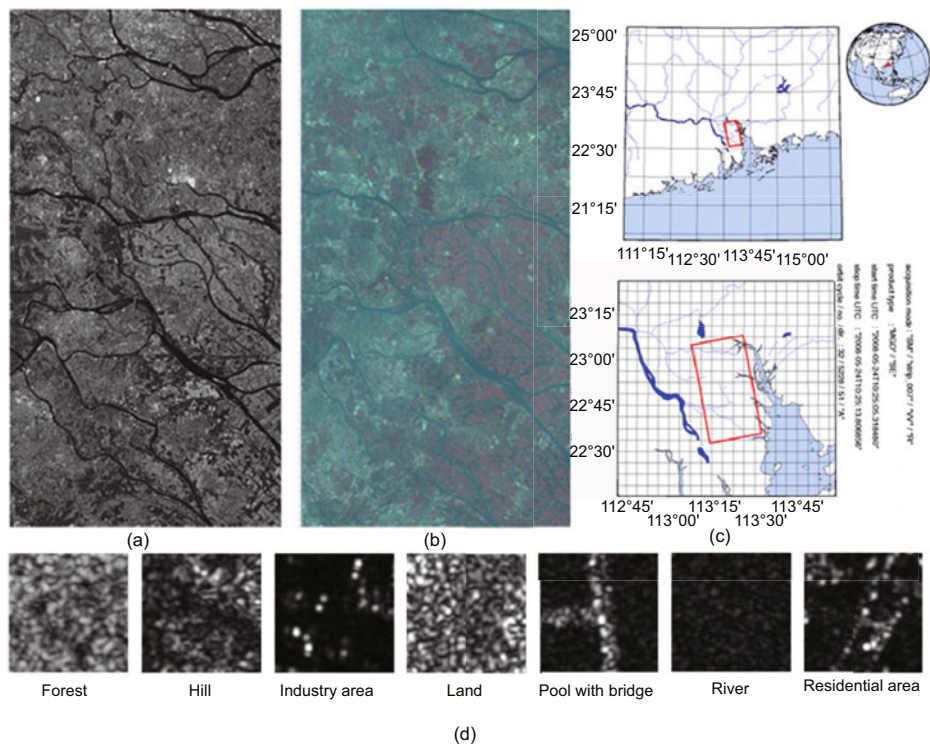
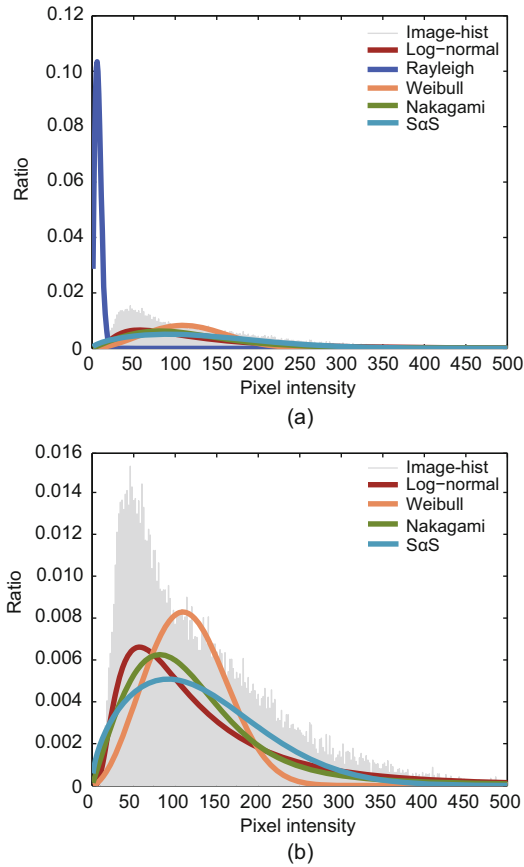


Fig. 3 TerraSAR-X images for experiments: (a) original SAR image; (b) ordinary optics image of the SAR image; (c) opposition of the SAR image in the Earth; (d) samples from the original SAR image



**Fig. 4** Histograms of the image and different distributions with (a) or without (b) Rayleigh. References to color refer to the online version of this figure

among log-normal (El), Nakagami (En), S $\alpha$ S (Es), Weibull (Ew), Rayleigh (Er), and the combinations of two or more distributions in grid pattern G1. For each  $N$ , we recorded the average accuracy. Table 2 shows the effect of different  $N$ 's on the classification results. As we can see, for a single estimator, several distributions provide poor classification accuracy. The strategies of combining different estimators are significantly better and more stable than using a single estimator, which means that one estimator can cover the shortage of another one. When  $N=4$ , the average accuracy is much better than that in other cases. According to Fig. 5, the combination of estimators (El+En+Es+Ew) performs best in the classification tasks. Therefore, the distributions we chose are log-normal, Nakagami, S $\alpha$ S, and Weibull.

In the gridding procedure, different sizes of the grid represent different amounts of information. However, it does not mean that a larger window brings a better result. In fact, a small window contains less information while a too large window seems

**Table 2** Classification accuracy as a function of the number of distributions

Number of distributions	Accuracy (%)	Error range (%)
1	79.86	6.08
2	83.54	2.50
3	84.29	1.65
4	<b>84.77</b>	0.65
5	84.57	0

The bold number indicates the best result

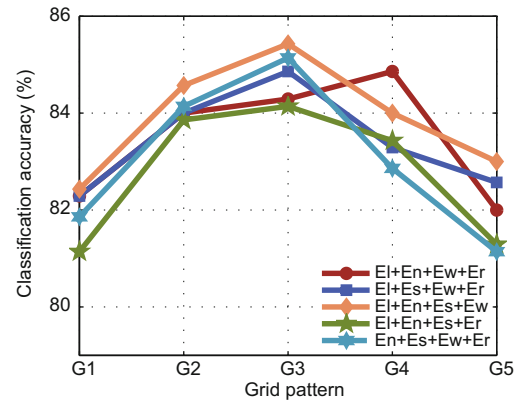


**Fig. 5** Classification accuracy of different combinations among estimators (El: log-normal; En: Nakagami; Es: S $\alpha$ S; Ew: Weibull; Er: Rayleigh)

rough. To determine a proper window size, we usually chose odd numbers as the patch size, such as  $5 \times 5$ ,  $7 \times 7$ , and  $9 \times 9$ . Fig. 6 shows that window G3 provides the highest classification rate, which means that window G3 with a larger size is appropriate for local estimation in SAR images. G4 including three windows can keep the spatial information, and provides a more stable result. G5 achieves the poorest performance due to its lack of scale information, and thus cannot represent the distribution information of the local sub-block best. More window sizes for SAR image interpretation will be explored in our future work. In the following comparative experiments, we chose G3 and El+En+Es+Ew respectively for s-texton feature generation. Then textons (or clustering centers) were obtained in C-Block, and feature vectors with  $1 \times 300$  dimension from histogram counting were classified by a  $K$ -nearest neighbor (KNN) method.

### 4.3 Feature setup for comparison

The performance of the s-texton feature has been compared with those of four well-founded feature extraction techniques: GLCM (Xie, 2008), Gabor, GMRF, and DSEM\_MRF (Krylov et al., 2009;



Voisin et al., 2010).

**GLCM:** GLCM used in this experiment has eight gray levels and four texture statistics (contrast, correlation, energy, and homogeneity), which are combined to a texture descriptor for classification.

**Gabor:** Images are filtered by a Gabor filter bank, and then the mean and variance computed from each filtered image are combined into a feature vector. Since eight orientations of three-level Gabor filters are used in this study, the dimension of the feature vector is  $1 \times 48$ .

**GMRF:** Parameters of GMRF modeling of the SAR image are estimated. Then statistics are executed respectively with each parameter, resulting in the corresponding statistic vectors to represent the image.

**DSEM\_MRF:** A DSEM approach is used to model the SAR amplitude PDF. Combine DSEM and MRF to compute the class-conditional probability for each pixel of the SAR image. Then the

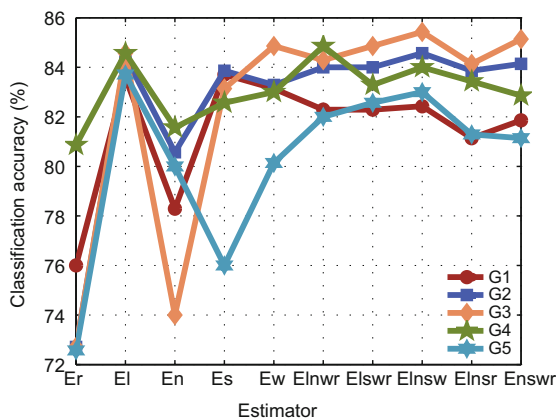


**Fig. 6** Classification accuracy of different grid patterns (G1:  $5 \times 5$ ; G2:  $9 \times 9$ ; G3:  $13 \times 13$ ; G4:  $7 \times 7$ ,  $9 \times 9$ , and  $11 \times 11$ ; G5: left-up, left-down, right-up, and right-down. El: log-normal; En: Nakagami; Es: S $\alpha$ S; Ew: Weibull; Er: Rayleigh)

SAR image is divided into 16 sub-blocks and the average of the class-conditional probability vectors is computed for each sub-block to produce a new vector. Subsequently, the vectors derived from the 16 sub-blocks are cascaded to describe the SAR images.

#### 4.4 Classification performance of s-texton and other features

Table 3 lists the experimental results of different descriptors. The s-texton feature approach obtains the highest classification accuracy in most classes, and outperforms Gabor, GLCM, DSEM\_MRF, and GMRF by 31.29%, 29.14%, 15.14%, and 5.43%, respectively. The superiority of the s-texton feature approach can be attributed to three aspects. First, regarding the method of pre-processing, the s-texton feature approach exploits directly the log-likelihood to choose a proper distribution for the following stages. Second, different sizes or patterns of the grid are chosen. These grids contain neighborhoods of each pixel, so the feature vectors extracted from them express the spatial information. Third, instead of filtering in the traditional texton algorithm, the parameters of different statistical distributions are combined to strengthen the local statistical information, and therefore the s-texton feature is applicable to different texture images.

## 5 Conclusions

In this paper, a statistical (s-texton) distribution feature has been proposed for SAR image classification. The statistical estimation methods have been used instead of filtering operation, and different estimators have been applied in the parameter estimation process. Experiments have been conducted to evaluate the classification performances of different estimators and grid patterns in the

**Table 3** Classification accuracy of the s-texton approach and other published approaches

Approach	Classification accuracy (%)							
	Forest	Hill	Industry	Farmland	Pool	River	Residential	Average
Gabor	49.00	54.00	46.00	43.00	79.00	59.00	49.00	54.14
GLCM	46.00	41.00	42.00	54.00	86.00	72.00	53.00	56.29
DSEM_MRF	82.00	57.00	38.00	74.00	83.00	<b>100.00</b>	58.00	70.29
GMRF	79.00	76.00	61.00	<b>75.00</b>	99.00	99.00	71.00	80.00
s-texton	<b>93.00</b>	<b>93.00</b>	<b>68.00</b>	72.00	<b>100.00</b>	<b>100.00</b>	<b>72.00</b>	<b>85.43</b>

Bold numbers indicate the best results

proposed method, and the classification results showed the superiority of using the s-texton feature. For future work we will explore and apply more appropriate estimators and window sizes for SAR image interpretation.

## References

- Benboudjema, D., Tupin, F., 2013. Markovian modelling and Fisher distribution for unsupervised classification of radar images. *Int. J. Remote Sens.*, **34**(22):8252-8266. <https://doi.org/10.1080/01431161.2013.827340>
- Fukuda, S., 2004. Relating polarimetric SAR image texture to the scattering entropy. Proc. IEEE Int. Geoscience and Remote Sensing Symp., p.2475-2478. <https://doi.org/10.1109/IGARSS.2004.1369795>
- Gambini, J., Mejail, M.E., Jacobo-Berlles, J., et al., 2006. Feature extraction in speckled imagery using dynamic B-spline deformable contours under the  $\mathcal{G}^0$  model. *Int. J. Remote Sens.*, **27**(22):5037-5059. <https://doi.org/10.1080/01431160600702616>
- He, C., Ahonen, T., Pietikainen, M., 2008. A Bayesian local binary pattern texture descriptor. Proc. 19th Int. Conf. on Pattern Recognition, p.1-4. <https://doi.org/10.1109/ICPR.2008.4761100>
- He, C., Li, S., Liao, Z., et al., 2013. Texture classification of PolSAR data based on sparse coding of wavelet polarization textons. *IEEE Trans. Geosci. Remote Sens.*, **51**(8):4576-4590. <https://doi.org/10.1109/TGRS.2012.2236338>
- Krylov, V., Moser, G., Serpico, S.B., et al., 2008. Modeling the Statistics of High Resolution SAR Images. Research Report RR-6722, INRIA, France.
- Krylov, V., Moser, G., Serpico, S.B., et al., 2009. Dictionary-based probability density function estimation for high-resolution SAR data. Proc. IS&T/SPIE Electronic Imaging, p.72460S.1-72460S.12. <https://doi.org/10.1117/12.816102>
- Krylov, V.A., Moser, G., Serpico, S.B., et al., 2013. On the method of logarithmic cumulants for parametric probability density function estimation. *IEEE Trans. Image Process.*, **22**(10):3791-3806. <https://doi.org/10.1109/TIP.2013.2262285>
- Kuruoglu, E.E., Zerubia, J., 2000. Modelling SAR with a generalisation of the Rayleigh distribution. *IEEE Trans. Image Process.*, **13**(4):527-533.
- Kuruoglu, E.E., Zerubia, J., 2003. Skewed  $\alpha$ -stable distributions for modelling textures. *Patt. Recog. Lett.*, **24**(1-3):339-348. [https://doi.org/10.1016/S0167-8655\(02\)00247-7](https://doi.org/10.1016/S0167-8655(02)00247-7)
- Leung, T., Malik, J., 2001. Representing and recognizing the visual appearance of materials using three-dimensional textons. *Int. J. Comput. Vis.*, **43**(1):29-44. <https://doi.org/10.1023/A:1011126920638>
- Oliver, C.J., 1986. A model for non-Rayleigh scattering statistics. *Opt. Acta: Int. J. Opt.*, **31**(6):701-722. <https://doi.org/10.1080/713821561>
- Oliver, C.J., Quegan, S., 2004. Understanding Synthetic Aperture Radar Images. SciTech Publishing, Stevenage.
- Schmid, C., 2001. Constructing models for content-based image retrieval. Proc. IEEE Computer Society Conf. on Computer Vision and Pattern Recognition, p.39-45. <https://doi.org/10.1109/CVPR.2001.990922>
- Silveira, M., Heleno, S., 2009. Separation between water and land in SAR images using region-based level sets. *IEEE Geosci. Remote Sens. Lett.*, **6**(3):471-475. <https://doi.org/10.1109/LGRS.2009.2017283>
- Singh, J., Datcu, M., 2013. SAR image categorization with log cumulants of the fractional Fourier transform coefficients. *IEEE Trans. Geosci. Remote Sens.*, **51**(12):5273-5282. <https://doi.org/10.1109/TGRS.2012.2230892>
- Spigai, M., Tison, C., Souyris, J.C., 2011. Time-frequency analysis in high-resolution SAR imagery. *IEEE Trans. Geosci. Remote Sens.*, **49**(7):2699-2711. <https://doi.org/10.1109/TGRS.2011.2107914>
- Varma, M., Zisserman, A., 2002. Classifying images of materials: achieving viewpoint and illumination independence. Proc. European Conf. on Computer Vision, p.255-271. [https://doi.org/10.1007/3-540-47977-5\\_17](https://doi.org/10.1007/3-540-47977-5_17)
- Varma, M., Zisserman, A., 2005. A statistical approach to texture classification from single images. *Int. J. Comput. Vis.*, **62**(1-2):61-81. <https://doi.org/10.1007/s11263-005-4635-4>
- Voisin, A., Moser, G., Krylov, V.A., et al., 2010. Classification of very high resolution SAR images of urban areas by dictionary-based mixture models, copulas and Markov random fields using textural features. Proc. SPIE Remote Sensing, p.585-599. <https://doi.org/10.1117/12.865023>
- Xie, X., 2008. A review of recent advances in surface defect detection using texture analysis techniques. *Electron. Lett. Comput. Vis. Image Anal.*, **7**(3):1-22.
- Yonezawa, C., Watanabe, M., Saito, G., 2012. Polarimetric decomposition analysis of ALOS PALSAR observation data before and after a landslide event. *Remote Sens.*, **4**(8):2314-2328. <https://doi.org/10.3390/rs4082314>